Polyhedron 37 (2012) 27–34

Contents lists available at SciVerse ScienceDirect

Polyhedron

journal homepage: www.elsevier.com/locate/poly

Tailoring antibacteria agents: Sulfonamide-based dinuclear and 1D polymer Cu(II) complexes

Jean-Bernard Tommasino [a,*], Guillaume Pilet [a], François N.R. Renaud [b], Ghénadie Novitchi [a], Vincent Robert [c,*], Dominique Luneau [a]

[a] Université de Lyon, Laboratoire des multiMatériaux et Interfaces, UMR 5615 CNRS, Université Claude Bernard Lyon 1, avenue du 11 novembre 1918, 69622 Villeurbanne Cedex, France
[b] Université de Lyon, UMR 5510 CNRS MATEIS, I2B Nosoco.tech®, Université Claude Bernard Lyon 1, avenue du 11 novembre 1918, 69622 Villeurbanne Cedex, France
[c] Laboratoire de Chimie Quantique, Institut de Chimie, UMR 7177 CNRS, Université de Strasbourg, 4 rue Blaise Pascal, B.P. 1032, F-67070 Strasbourg Cedex, France

ARTICLE INFO

Article history:
Received 2 December 2011
Accepted 27 January 2012
Available online 21 February 2012

Keywords:
Sulfonamide ligands
Cu(II) complexes
Antibacterial agents

ABSTRACT

Starting from two bioactive sulfonamide-based ligands (HL1: 4-amino-*N*-(2,6-dimethoxy-4-pyrimidinyl) benzenesulfonamide; HL2: 4-amino-*N*-(4-methyl-2-pyrimidinyl)benzenesulfonamide) and Cu(II) salts ($[Cu_2(Ac)_4]$ and $CuCl_2$, Ac = acetate), the synthesis of $[Cu_2(Ac)_2(L1)_2]$ (**1**) and $[Cu_2(L2)_4]$ (**2**) and $\{Cu(L1)_2(bipy)\}_n{\cdot}2nH_2O{\cdot}n(CH_3OH)$ (**1′**) (bipy = 4,4′-bipy) architectures with potential antibiotic and antiseptic activities is reported. To confirm the possibility to fulfill specific criteria and ultimately combine both properties, the bioactive sulfonamide-based complexes are structurally, electrochemically and magnetically characterized. Depending on the synthesis conditions, the Cu:sulfonamide stoichiometry and Cu···Cu communication are first varied by controlling the chemical nature of the ancillary ligand (Ac or bipy). Then, electrochemistry data support the stability of **1** and **2** dinuclear complexes, and **1′** 1D polymer, a prerequisite for their bioactivity in solution. Interestingly, the synthesis leads to architectures where the (SO_2-Ph-NH_2) moiety which is responsible for the antibacterial activity remains non-coordinated in the vicinity of Cu(II) antiseptic ions. Magnetic susceptibility measurements combined to multireference wavefunction *ab initio* calculations evidence a rather strong antiferromagnetic behavior in the dinuclear compounds ($H = -2JS_1S_2$, $2J_1 = -307.8$ cm^{-1} in **1**, $2J_2 = -63.2$ cm^{-1} in **2**) whereas chain **1′** is paramagnetic. The cooperativity quantified by the hopping integral which is available from the *ab initio* calculations of the exchange coupling constant is reduced by a factor of two when the number of sulfonamide ligands increases in complexes **1** and **2**. In contrast, it is negligibly small in the 1D polymer **1′**. These characterized bioactive sulfonamide-based Cu(II) compounds appear as promising targets, complying with the structural and electronic expectations for antibacterial and antiseptic purposes. Finally, the antibacterial activity studies question the prerequisite for cooperative metal centers to rationally design antibacterial agents since the minimum inhibitory concentration in the paramagnetic chain **1′** is greatly reduced as compared to antiferromagnetic complexes **1** and **2**.

1. Introduction

Since the need for commercial bioactive mixed organic–metal compounds continuously increases, the synthesis of such systems has become of prime importance [1]. In this respect, hybrid metal–sulfonamide complexes have received much attention, knowing that the pharmacological activity of the organic moieties is often enhanced by complexation with metal ions [2–4]. Evidently, one would like to combine the ligand and metal ion properties (antibiotic and antiseptic, respectively) to produce a single entity exhibiting simultaneously both therapeutic activities. To reach this challenging goal, some specific conditions must be fulfilled in the light of recent experimental observations [5–8]. First, it has been shown that the nuclearity of Cu(II) complexes is determinant in the oxidative DNA cleavage [6]. Polynuclear complexes are indeed more efficient than their monomer analogs, a possible consequence of metal–metal interactions. Then, any organic modification of the R moiety (see Fig. 1) of the sulfonamide skeleton is generally incompatible with the presence of a *p*-amino group which is responsible for the therapeutic activity. Indeed, the use of bacterial enzyme inhibitors such as sulfonamide as bridging ligands has not been much reported in the literature. In order to facilitate the coordination to metal ions centers, it is necessary to functionalize the sulfonamide molecule. By varying the nature of the R substituent (see Fig. 1), the coordination character of the sulfonamide is enhanced as a consequence of the greater lability of the R-NH-SO_2– proton.

* Corresponding authors.
E-mail addresses: jbtomasi@univ-lyon1.fr (J.-B. Tommasino), vrobert@unistra.fr (V. Robert).

0277-5387/$ - see front matter © 2012 Elsevier Ltd. All rights reserved.
doi:10.1016/j.poly.2012.01.025

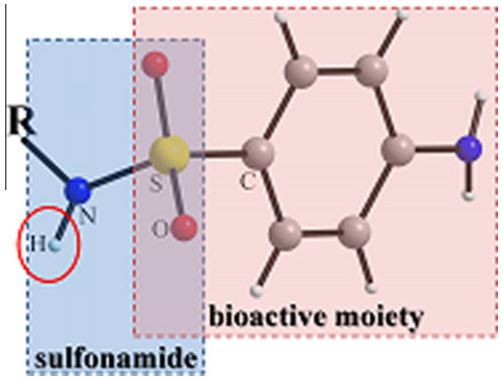

Fig. 1. Schematic representation of a sulfonamide involving the bioactive (SO_2-Ph-NH_2) moiety.

This synthetic strategy has contributed to the fast development of N-sulfinyl-based ligands involved in highly efficient asymmetric Cu(II) catalysts [9]. Therefore, to comply with these specifications (i.e., polymetallic and bioactive sulfonamide-type ligand), we felt that a new synthetic route to bind sulfonamide bioactive ligand to metal centers would be desirable. In particular, one would like to possibly control the metal:bio-ligand ratio within the complex, assuming that any ligand enrichment may modulate the antibiotic activity (Minimum Inhibitory Concentration, MIC). For a synergetic use, the latter should be comparable to the one of the bare sulfonamide species. One of the central issue is that the accumulation of sulfonamide ligands onto antiseptic dinuclear complexes is likely to alter the interactions between the metal ions. In order to meet these requirements, sulfonamide-based dinuclear Cu(II) complexes were considered as natural targets. The Cu(II) ion was chosen considering its recognized antiseptic activity and strong enough Lewis acid character to bind antibacteria soft sulfonamide bases. Monomers combining metal 3*d* have been recently characterized [10] by electrochemical measurements and single-crystal X-ray diffraction, a rather unexpected result considering that bioactive sulfonamide-based complexes are usually difficult to crystallize [11].

We herein report the synthesis and structure determinations of bioactive sulfonamide-based dinuclear complexes. Starting from the dinuclear precursor $[Cu_2(Ac)_4]\cdot 2H_2O$ where the Cu(II) ions are

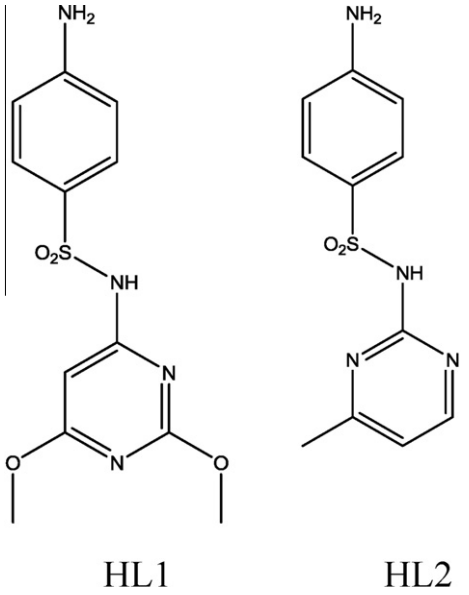

Fig. 2. HL1 and HL2 sulfonamide bioactive-ligands used in the elaboration of complexes **1**, **2** and **1′**.

known to effectively communicate as probed by a strong exchange coupling constant *ca.* $2J = -300\ cm^{-1}$ [12], sulfonamide ligands (HL1 = sulfadimethoxine and HL2 = sulfamerazine, see Fig. 2) were introduced to fabricate two new dinuclear complexes with Cu:sulfonamide stoichiometries 1:1 (**1**) and 1:2 (**2**) and the 1D polymer analog **1′**. The use of bipyridine as a spacer allows one to reduce the cooperativity between the Cu(II) ions and to assess the reported bioactivity/cooperativity correlation [6c].

Electrochemical studies were performed to control the complexes stability in solution. The accessibility of the bioactive organic part (see Fig. 1) within the complexes was evidenced by X-ray crystal structures, while the magnetic susceptibility was measured and used to probe the metal–metal interaction through the exchange coupling constant modulation. Finally, multireference wavefunction-based *ab initio* calculations were carried out to extract the effective resonance integral between the Cu(II) centers and to highlight the expected cooperativity. This work is to be considered as a first step in the preparation and investigation of multisite bioactive complexes.

2. Experimental details

2.1. Synthesis

2.1.1. $[Cu_2Ac_2(L1)_2]\cdot 2CH_3CN$ (**1**)

Copper acetate salt (0.5 mmol) and the HL1 bioactive sulfonamide ligand (1 mmol) were dissolved separately in 5 mL of CH_3CN. Then, the blue copper acetate solution was introduced drop wise to the colorless HL1 solution and a green solution was obtained. The latter was stirred for 10 min and after 1 week of slow evaporation of the solvent at room temperature, green single-crystals (suitable for X-ray data characterizations) were grown. *Anal.* Calc. for $C_{28}H_{32}Cu_2N_8O_{12}S_2$: C, 38.93; H, 3.73; Cu, 14.71; N, 12.97; O, 22.23; S, 7.42. Found: C, 39.31; H, 3.43; Cu, 14.52; N, 12.80%. IR, ν_{max} (cm^{-1}): 3371 $\nu^{as}(NH_2)$, 1571 νC=O, 1148 $\nu(SO_2)$, 1071 $\nu(SO_2)$, 771 ν(S–N).

2.1.2. $[Cu_2(L2)_4]\cdot(MeOH)\cdot 0.3H_2O$ (**2**)

To a methanolic solution (5 mL) of copper acetate salt (0.50 mmole), a methanolic solution of the bioactive HL2 sulfonamide ligand (sulfamerazine, 1.26 mmole) was added at room temperature. After 3 min of stirring, a concentrated solution of NH_3 (25% volume) was added drop wise until the apparition of an intense blue color characteristic of the presence of the $[Cu(NH_3)_6]^{2+}$ complex. After few days, the solution color turned to green and single-crystal for X-ray characterizations were obtained by slow evaporation of the solvent. *Anal.* Calc. for $C_{44}H_{44}Cu_2N_{16}O_8S_4$: C, 44.78; H, 3.76; Cu, 10.77; N, 18.99; O, 10.84; S, 10.87. Found: C, 44.72; H, 3.81; Cu, 10.64; N, 18.92. IR, ν_{max} (cm^{-1}): 3358, $\nu^{as}(NH_2)$, 1594 νNH_2/C–C(Ph), 669 ν(C–S), 1269 $\nu(SO_2)$, 1073 $\nu(SO_2)$, 881 ν(S–N).

2.1.3. $\{Cu(L1)_2(bipy)\}_n\cdot 2nH_2O\cdot nCH_3OH$ (**1′**)

The same procedure was used as for **2** with $Cu(ClO_4)_2\cdot 2H_20$ (0.50 mmole, 146 mg)/3 equiv. of 4,4′-bypiridin (1.5 mmole, 235 mg)/1.2 equiv. of sulfadimethoxine (L1H, 0.60 mmole, 186 mg). Single green crystals were obtained.

Anal. Calc. for $C_{34}H_{34}Cu_1N_{10}O_8S_4$: C, 48.71; H, 4.09; Cu, 7.58; N, 16.71; O, 15.27; S, 7.65. Found. C, 48.72; H, 4.11; Cu, 7.64; N, 16.92.IR, ν_{max} (cm^{-1}): 3351 $\nu^{as}(NH_2)$, 1591 $\nu(NH_2/C–C(Ph))$, 684 ν(C–S), 1255 $\nu(SO_2)$, 1070/1126 $\nu(SO_2/C–C(Ph)$, 856 ν(S–N).

2.2. Electrochemistry

Solvents and reagents were obtained commercially (Aldrich) and used without further purification. Electrochemical measure-

ments were performed using an AMEL 7050 all-in one potentiostat, using a standard three-electrode setup with a glassy carbon electrode, platinum wire auxiliary electrode and SCE (saturated calomel electrode) as the reference electrode. The complex solutions in DMSO were 1.0 mM, 2 mM and 0.1 M in the supporting electrolyte n-Bu_4NPF_6. Under these experimental conditions, the ferrocene/ferricinium couple, used as an internal reference for potential measurements, was located at $E_{1/2}$ = 0.421 V.

2.3. X-ray crystallography

Single-crystal X-ray diffraction measurements were recorded upon the structures of the three original complexes. Diffraction data sets were collected on an Oxford diffractometer equipped with a CCD camera and the related softwares [13]. An absorption correction (multi-scan [14] or analytical [15]) was applied to all the data. The structures were solved by direct methods using the SIR97 program [16] combined to Fourier difference synthesis and refined against F or F^2 and using the CRYSTALS program [17]. In each structure, all atomic displacements for non-hydrogen atoms were refined anisotropically. Hydrogen atoms belonging to carbon atoms were located theoretically while the others (belonging to oxygen atoms) by Fourier Difference but refined using a *riding* method.

2.4. Magnetic susceptibility measurements

Magnetic susceptibility data (2–300 K) were collected on powdered polycrystalline samples by SQUID magnetometer on Quantum Design model MPMS instrument under an applied magnetic field of 0.1 T dependencies. Magnetization isotherm was collected at 2 K between 0 and 5 T. All data were corrected for the contribution of the sample holder and diamagnetism of the samples estimated from Pascal's constants [18]. The analysis of the magnetic data was carried out by simultaneous $\chi_M T$ and $\chi_M(T)$ thermal dependencies including temperature-independent paramagnetism (*TIP*), impurity contribution (ρ), and intermolecular interaction (zJ).

The minimization was carried out with an adapted version of *Visualiseur-Optimiseur* for Matlab® [19,20] using nonlinear least-square Lavenberg–Marquard algorithm.

2.5. Computational details

It is known that some care must be taken to properly define energy spectrum of open-shell systems [21]. However, spectroscopic accuracy can be reached using complete active space self-consistent field (CASSCF) and subsequent correlation effects treatments. Indeed, the CASSCF method gives reasonable electron distribution and accounts for the leading electronic configurations. From the d^9 electronic configuration of Cu(II) ion, CAS[2,2]SCF (i.e., two electrons in two molecular orbitals, MOs) calculations were first performed upon a simplified structure of complexes **1** and **2**. To reduce the computational cost, each *p*-aminobenzyl group of the four ligands was changed into hydrogen atoms with adapted C–H bond distances. It has been shown that chemical changes which maintain the nature of the bridging ligands and the polarization properties of the coordination spheres are unlikely to deeply modify the exchange coupling intensity. These CASSCF calculations were performed using the MOLCAS7.2 package [22]. All atoms were described using ANO RCC-type atomic functions [23]. Carbon, nitrogen, oxygen, and sulfur atoms were described with DZP-type contractions, whereas a (21s15p10d6f4g2h)/[5s4p2d1f] contraction was used for the copper atom. Finally, the hydrogen atoms were depicted using a minimal basis set contraction (8s4p3d1f)/[1s]. Whatever the definition of the active space, it has been clearly demonstrated that the exchange interaction cannot be accurately evaluated ignoring the dynamical correlation phenomena. For a given geometry, the dynamical polarization and correlation effects were then included using the Difference Dedicated Configuration Interaction (DDCI) method as implemented in the CASDI code [24]. As the number of degrees of freedom (i.e., holes in doubly occupied MOs, particles in virtual MOs of the CASSCF wavefunction) increases, one generates the successive DDCI-1, DDCI-2 and DDCI-3 CI spaces as discussed in the literature for related compounds [25]. To eliminate the arbitrariness of the set of MOs in the DDCI calculations, natural orbitals were first generated by averaging the DDCI-1 density matrices of the singlet and triplet states. This procedure was iterated until convergence upon the energies. DDCI-3 calculations were performed using the resulting set of MOs.

2.6. Antibacterial study: determination of minimum inhibitory concentrations (MICs) of bioactive-ligands and their complexes by agar dilution

The bioactive ligands HL1, HL2 and complexes **1**, **2**, **1′** have been tested according to the European Committee for antimicrobial susceptibility testing (EUCAST: European Society of Clinical Microbiology and Infectious Disease). The different products were dissolved in 20% concentration of DMSO (dimethyl sulfoxide) at concentrations ranging from 5 to 1280 mg L^{-1}. Then, 18 mL of molten agar (Mueller Hinton agar II, bioMérieux, Lyon, France) were added to 2 mL of the different concentrations. The concentrations were adjusted from 0.5 to 128 mg L^{-1} with a final DMSO concentration of 2% which has no inhibitory effect on bacterial growth. The tested bacterial strains is *Enterococcus faecalis* (clinical strain from Nosoco. tech® collection. Number 20.7). Plates were incubated 18–24 h at 37 °C. The MIC is defined as the lowest agent concentration that fully inhibits visible growth as judged by the naked eye.

3. Results and discussion

Complexes $[Cu_2Ac_2(L1)_2]\cdot 2(CH_3CN)$ (**1**), $[Cu_2(L2)_4]\cdot(MeOH)\cdot 0.3\,H_2O$ (**2**) and $\{Cu(L1)_2(bipy)\}_n\cdot 2nH_2O\cdot nCH_3OH$ (**1′**) were obtained by ligand exchange reaction between Cu(II) salts and respective sulfonamide (HL1 for **1** and **1′**; HL2 for **2**) in the presence of NH_3(aq) 25% in water solution [11]. Let use mention that the use of other bases such as NaOH, KOH or triethylamine in any molar ratio was not successful. This suggests the special role of ammonium solution in the formation of complexes based on bioactive sulfonamide ligands. Thus, from our observations, the first step should be the formation of a $[Cu(NH_3)_6]^{2+}$ complex evidenced by the blue intense color of the solution [11]. This intermediate complex reacts progressively with the sulfonamide ligand (HL1 or HL2) to produce the complexes **1**, **2** and monodimensional polymer **1′**. Following this original synthesis method, **1**, **2** and **1′** were isolated with significant yields (*ca.* 70%) and fully characterized (see Tables 1A and 1B).

Due to multiple donor atoms in the sulfonamide moiety, different coordination modes to metal centers have been reported in the literature (see Fig. 3) [8]. In complexes **1** and **2**, the deprotonated sulfonamide bioactive ligands $L1^-$ and $L2^-$ adopt a coordination mode IV (see Fig. 3) once connected to the Cu(II) metal centers resulting in dinuclear complexes (see Fig. 4).

In both complexes, the environment of the two metal Cu(II) ions is the same with a regular X_4 square plane (X = N or O; N_2O_2 for **1** and N_4 for **2**) where the Cu–X bond lengths range from 1.966(3) to 2.023(3) Å (X = N or O; average: 2.00 Å) for **1**, from 1.997(4) to 2.048(4) Å (X = N; average: 2.02 Å) for **2**. This metal environment is completed by oxygen atoms belonging to SO_2 ligand moiety as second coordination sphere: one oxygen atom per Cu(II) within **1**

Table 1A
Details of the data collections and refinements.

	1	**2**	**1′**
Ref. formula	$C_{32}H_{38}Cu_2N_{10}O_{12}S_2$	$C_{45}H_{48.66}Cu_2N_{16}O_{9.33}S_4$	$C_{35}H_{42}Cu_1N_{10}O_{11}S_2$
FW (g mol^{-1})	945.9	1218.3	906.5
Crystal system	triclinic	monoclinic	monoclinic
Space group	$P\bar{1}$	$C2/c$	$P2/n$
a (Å)	8.332(1)	39.949(1)	18.059(1)
b (Å)	9.911(1)	12.5809(3)	11.0588(6)
c (Å)	13.092(2)	20.8751(6)	20.509(1)
α (°)	98.99(1)	90	90
β (°)	106.82(1)	101.352(3)	98.047(6)
γ (°)	98.06(1)	90	90
V (Å^3)	1002.4(2)	10286.3(5)	4055.4(4)
Z	1	8	4
T (K)	100	293	293
D (g cm^{-3})	1.567	1.573	1.485
μ (mm^{-1})	1.237	1.062	0.713
Independent reflections	4640	10 163	7042
R_{int}	0.059	0.039	0.039
$R(F)/R_w(F)$	0.0483/0.0556	0.0611/0.0629	0.0555/0.0764
S	1.06	1.13	1.05
Number of Reflections	3135	6662	7037
Number of parameters	262	675	538
$\Delta\rho_{max}/\Delta\rho_{min}$ (e Å^{-3})	1.39/−1.18	1.35/−2.13	0.59/−0.54
Absorption correction	analytical	multi-scan	multi-scan

(average Cu–O bond lengths equals to 2.47 Å) and two oxygen atoms per Cu(II) within **2** (average Cu–O bond lengths equals to 2.59 Å). Fixing z as the internuclear axis, such environment leaves one unpaired electron in a $d_{x^2-y^2}$-type orbital upon each Cu(II) center. The relative orientation of the coordination spheres suggest a δ-type overlap between the magnetic Cu(II) orbitals. The Cu···Cu distances are relatively short for both complexes (2.57 and 2.60 Å for **1** and **2**, respectively). The crystal packing is maintained by hydrogen bonds between the dimers and non-coordinated solvent molecules (acetonitrile for **1** and methanol/water for **2**) forming a compact network.

The situation is rather different in **1′** which exhibits a 1D polymer structure (see Fig. 5) with chains running along the *b*-axis of the unit-cell. The chelating mode III (see Fig. 3) is observed once the deprotonated $L1^-$ ligand is connected to the Cu(II) metal ion.

The Cu(II) cation is located in a N_6 distorted octahedral environment with four short (2.00 Å) and two long (2.67 Å) Cu–N bond lengths. The former involve the nitrogen atoms belonging to the two deprotonated bioactive ligands. Such arrangement gives rise to chains characterized by Cu···Cu distances equal to 11.06 Å. The structural cohesion is obtained by hydrogen bonds between chains and co-crystallized solvent molecules (water and/or methanol).

To complement the solid state characterization, the stability of these three original complexes in solution was checked using electrochemical measurements performed in DMSO. It has been shown that the HL1 and HL2 bioactive sulfonamide ligands exhibit an irreversible oxidation step (1.23 and 1.20 V, see Table 2) [11]. Their corresponding dinuclear complexes **1** and **2**, and chain **1′** display a similar wave 1.30, 1.35 and 1.29 V, respectively (see Table 2). The latter was assigned to the oxidation of the terminal $-NH_2$ group of the sulfonamide ligand [11]. This result suggests that the amine group of the organic moiety responsible for the therapeutic effects remains non-coordinated to metal ion within the complexes.

During the reduction process in Fig. 6, the voltammograms of **1** and **2** are characterized by two steps with the same relative intensity: a quasi-reversible large wave (−0.19 and −0.45 V for **1** and **2**, respectively) followed by an irreversible peak (−1.80 and −2.10 V for **1** and **2**, respectively). These irreversible peaks are related to typical redissolution oxidation peaks (Table 2 and Fig. 6). The general patterns of the voltammograms of all complexes remained unchanged for hours, suggesting that there is no degradation of the dimer entities in solution. Moreover, the cyclic voltammetry

Table 1B
Selected bond lengths (Å) and bond angles (°).

*Complex **1***			
Cu1–N11	2.023(3)	Cu1–N21	1.991(3)
Cu1–O34	1.966(3)	Cu1–O33	1.963(3)
N11–Cu–N21	172.2(1)	N11–Cu1–O34	88.2(1)
N11–Cu1–O33	91.1(1)	N21–Cu1–O33	88.8(1)
O34–Cu1–O33	170.0(1)		
*Complex **1′***			
Cu1–N8	2.727(3)	Cu1–N38	2.011(4)
Cu1–N31	1.986(3)	Cu1–N20	2.003(4)
Cu2–N24	1.999(4)	Cu2–N6	2.621(3)
Cu2–N9	1.976(3)	Cu2–N27	2.016(4)
N8–Cu1–N38	79.98(7)	N8–Cu1–N31	54.4(1)
N38–Cu1–N31	89.53(9)	N8–Cu1–N8	160.0(1)
N31–Cu1–N8	125.4(1)	N8–Cu1–N20	100.02(7)
N38–Cu1–N20	180	N31–Cu1–N20	90.47(9)
N31–Cu1–N31	179.1(2)	N6–Cu2–N24	98.28(7)
N6–Cu2–N9	56.0(1)	N24–Cu2–N9	91.26(9)
N6–Cu2–N6	163.4(1)	N9–Cu2–N6	123.6(1)
N9–Cu2–N9	177.5(2)	N6–Cu2–N27	81.72(7)
N24–Cu2–N27	180	N9–Cu2–N27	88.74(9)
*Complex **2***			
Cu1–N1	2.008(4)	Cu1–N21	2.014(4)
Cu1–N48	2.019(4)	Cu1–O51	2.601(4)
Cu1–N68	2.035(4)	Cu1–O71	2.633(4)
Cu2–N8	2.048(4)	Cu2–O30	2.570(4)
Cu2–O10	2.539(4)	Cu2–N41	1.986(4)
Cu2–N28	2.037(4)	Cu2–N61	1.997(4)
N1–Cu1–N21	178.5(2)	N1–Cu1–N48	91.1(2)
N21–Cu1–N48	90.3(2)	N1–Cu1–O51	93.7(2)
N21–Cu1–O51	86.3(2)	N48–Cu1–O51	60.4(2)
N1–Cu1–N68	88.7(2)	N21–Cu1–N68	90.2(2)
N48–Cu1–N68	161.9(2)	O51–Cu1–N68	137.6(1)
N1–Cu1–O71	90.5(2)	N21–Cu1–O71	88.0(2)
N48–Cu1–O71	138.3(2)	O51–Cu1–O71	77.9(1)
N68–Cu1–O71	59.8(1)	O10–Cu2–O30	76.1(1)
N8–Cu2–O10	61.0(2)	N28–Cu2–O30	60.7(1)
N8–Cu2–N28	162.1(2)	N8–Cu2–N41	89.6(2)
O10–Cu2–N28	136.9(1)	O10–Cu2–N41	90.1(2)
N8–Cu2–O30	137.1(2)	N28–Cu2–N41	90.6(2)
O30–Cu2–N41	89.4(2)	N28–Cu2–N61	91.1(2)
N8–Cu2–N61	88.9(2)	O30–Cu2–N61	91.1(2)
O10–Cu2–N61	88.4(2)	N41–Cu2–N61	178.3(2)

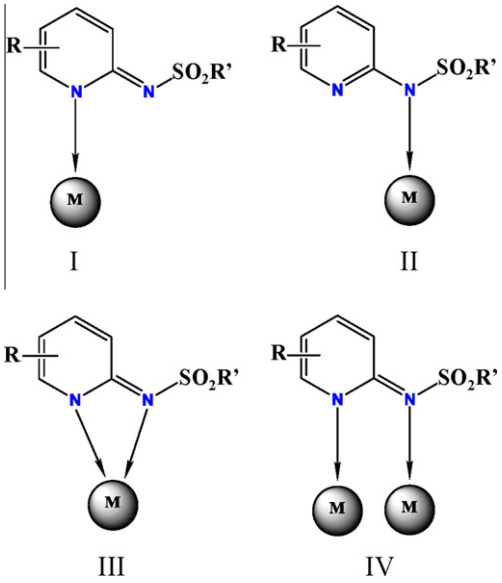

Fig. 3. Coordination modes of deprotonated sulfonamides (M: metal ion. R = alkyl; R′ = aromatic or alkyl groups).

of $[Cu_2(Ac)_4]$ salt performed in the same conditions is different from the ones recorded for **1** and **2** demonstrating again the complexes stability in solution. The coulometry on the first reduction step for **1** and **2** exhibits an electron apparent number value equal to 2 F/mole. Therefore, these processes correspond to the simultaneous Cu(II) → Cu(I) reduction of both metal centers within the complexes.

The scenario is contrasted in **1′** where both mono-electronic reduction steps (Cu(II) → Cu(I) and Cu(I) → Cu(0)) are irreversible, and followed by two peaks assigned to the 4,4′-bipy bridge reduction (Table 2). In conclusion, the ligand moiety (SO_2-Ph-NH_2) which is responsible for the antibacterial activity remains non-coordinated whatever the architecture. In both solid state and solution, such structural arrangement is a prerequisite to maintain the bioactivity of the ligands in the vicinity of the Cu(II) antiseptic ions.

The magnetic properties of compounds **1**, **2** and **1′** were then investigated by DC susceptibility measurements in the 2–300 K temperature range under a field of 0.1 T. Thermal evolution of magnetic susceptibility for both dinuclear complexes is given in Fig. 4. At room temperature, the χT values for **1** is 0.421 $cm^3\ K\ mol^{-1}$ which is smaller than the theoretical expected χT value (0.75 $cm^3\ K\ mol^{-1}$) for two non-interacting Cu(II) ions (d^9, $g = 2.0$, $S = 1/2$). With decreasing temperature, the χT product continuously decreases and finally reaches a value close to zero (0.011 $cm^3\ K\ mol^{-1}$) at 60 K. This behavior indicates the presence of a strong antiferromagnetic interaction. The value of χT at 300 K for **2** is 0.665 $cm^3\ K\ mol^{-1}$. Upon cooling, the χT product continuously decreases and reaches the value of 0.014 $cm^3\ K\ mol^{-1}$ at 7 K, suggesting antiferromagnetic interactions in **2**. In contrast, **1′** is essentially paramagnetic as a consequence of the introduction of the bipyridine spacer (see Fig. 7).

Using a $S = 1/2$ chain model for **1′** [26–30]:

$$H = -2J\sum S_i S_{i+1}$$

$$\chi(\alpha) = \frac{N_A g^2 \mu_B^2}{4|2J|T}\,\frac{1 + 0.08516\alpha^{-1} + 0.23351\alpha^{-2}}{1 + 0.73382\alpha^{-1} + 0.13696\alpha^{-2} + 0.53568\alpha^{-3}}$$

$$\alpha = \frac{kT}{|2J|}$$

a negligible $J_{1'} = 0.067\ cm^{-1}$ value ($g = 2.15$) was obtained, a feature of the absence of communication between the Cu(II) ions. These values are consistent with previously reported dinuclear and polymer Cu(II) connected by 4,4′-bipy-bridged [31,32]. According to

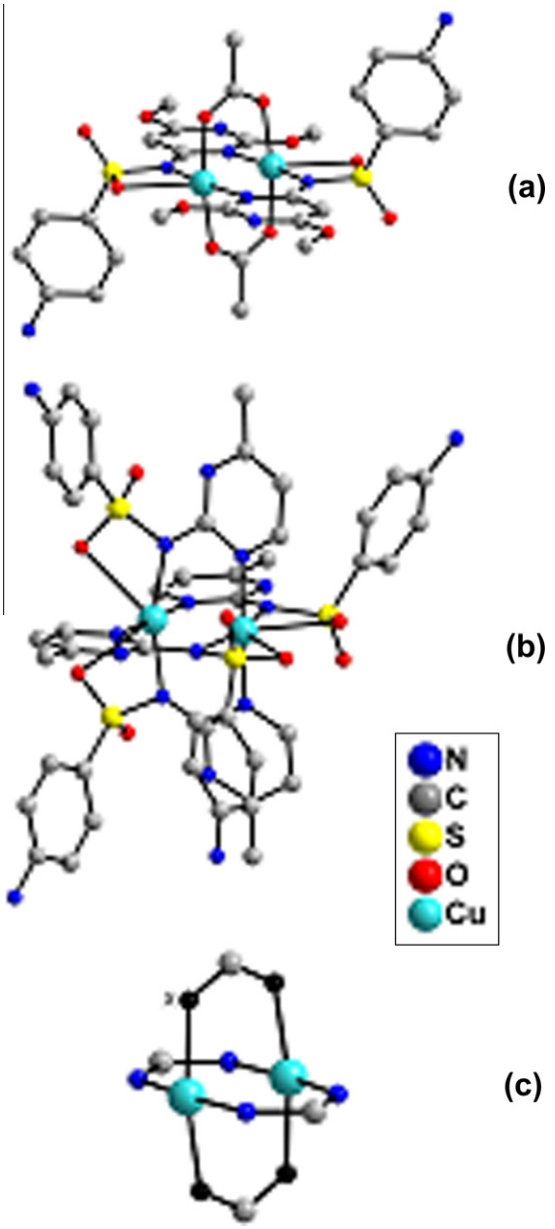

Fig. 4. Crystal structures of **1** (a) and **2** (b). For clarity, hydrogen atoms and non-coordinated solvent molecules have been removed; (c) simplified view of metal ion dimers with their organic bridges within **1** and **2** (X = O or N).

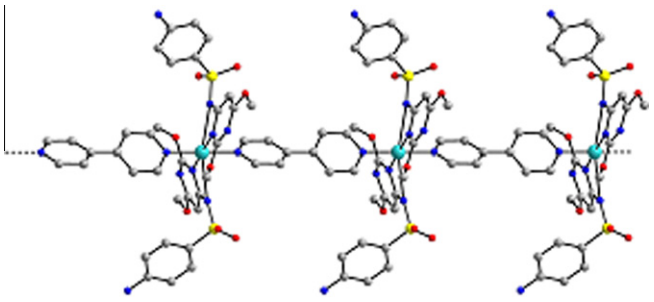

Fig. 5. Crystal structure of **1′** with chains running along the *b*-axis of the unit-cell. For clarity, hydrogen atoms and solvent molecules have been removed.

Table 2
Electrochemical data for HL1 and HL2 sulfonamide ligands, **1** and **2** dimers, and **1′** polymer. 4,4′-bipy data are introduced for comparison.

	Anodic	Cathodic			
HL1[d]	1.23[a]				−2.45[a]
HL2[d]	1.20[a]				−2.95[a]
$[Cu_2Ac_2]$		−0.40[b]	−1.30[b]		
4,4′-bipy				−1.92	−2.32
1	1.30[a]	−0.19[b]	−1.80		
2	1.35[a]	−0.45[b]	−2.10		
1′	1.29[a]	−0.22[b]	−1.66	−1.88[c]	−2.37[c]

Peak potentials (V) recorded in DMSO at 293 K with a glassy carbon electrode, 0.1 M n-Bu_4NPF_6 as supporting electrolyte; all potentials are vs. SCE, scan rate 0.1 V s^{-1}.
[a] Irreversible system.
[b] Quasi-reversible.
[c] Reduction of 4,4′-bipy in the complex.
[d] See Ref. [11].

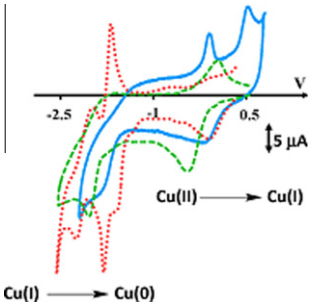

Fig. 6. Cyclic voltammetry of **1** (blue full line), **2** (green dashed line) and **1′** (orange dotted line) in reduction in DMSO using a glassy carbon electrode (3 mm diameter) at 100 mV/s. (Color online.)

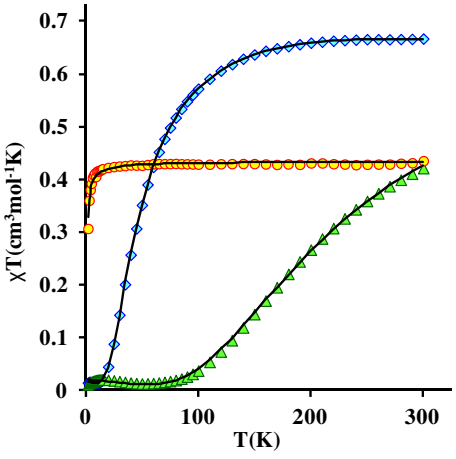

Fig. 7. χT vs. T plots data for **1** (green triangle), **2** (blue square) and **1′** (orange circle). The black lines correspond to the best fit according to dinuclear or chain models with parameters indicated in the text. (Color online.)

the isolated dinuclear structures of **1** and **2**, the magnetic properties can be analyzed using the isotropic spin Heisenberg Hamiltonian $H = -2JS_1S_2$ where $S_1 = S_2 = 1/2$, with the following analytical expression:

$$\chi_d = \frac{2Ng_{Cu}^2\beta^2}{kT}\frac{1}{3+e^{-2J/kT}}$$

The fitting procedure (see Fig. 7) leads to $J_1 = -153.9(7)\ cm^{-1}$, $\rho = 0.046(4)$, $g = 2.179(9)$, $zJ_1 = -0.001(2)\ cm^{-1}$ and $TIP = -1.84 \times 10^{-5}\ cm^3\ mol^{-1}$ for **1**; $J_2 = -31.60(2)\ cm^{-1}$, $\rho = 0.040(2)$, $g = 2.11(2)$, $zJ_2 = -0.02(2)\ cm^{-1}$ and $TIP = -1.84 \times 10^{-5}\ cm^3\ mol^{-1}$ for **2**, ($R = 4.08 \times 10^{-5}$ for **1**; R = 2.57×10^{-5} for **2**).

Table 3
Exchange coupling constants (cm^{-1}) and Cu–Cu distances (Å) for tetrakis aminobenzyl bridging dinuclear Cu(II) compounds.

Compound	Cu–Cu distance (Å)	$-2J$ (cm^{-1})	Reference
$[Cu_2(TzTs)_4]$	2.7859(5)	–	[33]
$[Cu_2(tz\text{-}tol)_4]$	2.722(1)	−121	[34]
$[Cu_2(stz)_4]$	2.671(2)	−61.5	[35]
$[Cu_2(tz\text{-}ben)_4]$	2.629(2)	−114.1	[5]
$[Cu_2(st\text{-}naf)_4]$	2.626(1)	−104	[34]
$[Cu_2(L2)_4]$ (**2**)	2.569(9)	−63.18	This work
$[Cu_2Ac_2(L1)_2]$ (**1**)	2,598(7)	−307.8	This work
$Cu_2Ac_4(H_2O)_2$	2.6143	−30	[12]
$[Cu_2(sulfameter)_4]$	2.556	–	[36]
$[Cu_2(PyBp)_4]$	2.5162(9)	−284	[37]
$[Cu_2Ac_2(L)_2]$	2.5412(6)	−216.7	[38]

tz-tol, *N*-(thiazol-2-yl)toluenesulfonamide; tz-naf, *N*-(thiozol-2-yl)naphthalenesulfonamide; stz, sulfathiazole; TzTs, *N*-thiazol-2-yl-(4-methylphenyl)sulfonamide; PyBp, *N*-(pyridin-2-yl)biphenyl-4-sulfonamide; Htz-ben, *N*-(thiazol-2-yl)benzenesulfonamide; sulfameter, 4-amino-*N*-(5-methoxy-2-pyrimidinyl)benzenesulfonamide; L, 4-amino-*N*-[4,6-domethyl-2-pyrimidyl]benzenesulfonamide.

As seen in Table 3 large variations (−308 to −61.5 cm^{-1}) of the exchange coupling constants have been observed in different dinuclear Cu(II) compounds holding similar bridging ligands [29–38]. To further inspect the magnetic properties in complexes **1** and **2**, *ab initio* calculations were performed. The parameters governing the exchange coupling constant $J = K - 2t^2/U$ are the effective direct exchange K, resonance integral t and on-site repulsion U which can be extracted from *ab initio* wavefunction calculations [39]. Clearly, the acetate fragment is an efficient and well recognized magnetic coupler. Since the super-exchange contributions are additive along the different channels characterized by the different hopping integrals t, the **L1** ligand turns out to be as efficient as the acetate ligand. Indeed, the exchange coupling constants of **1** and $Cu_2(Ac)_4{\cdot}2H_20$ are very similar in amplitude (see Table 3). The situation is evidently contrasted when ligand **L2** is involved. Thus, to further inspect the magnetic properties in complexes **1** and **2**, *ab initio* calculations were performed. From the paramagnetic behavior of **1′**, the resonance integral is expected to be vanishingly small, a signature of the low-cooperativity between the Cu(II) ions and we felt that calculations would not be instructive. For **1** and **2**, the active space includes the anticipated unpaired electrons and MOs of the system, leading to a CAS[2,2] (i.e., two electrons in two MOs) zeroth-order description. The system under study was simplified by leaving out atoms which belong at least to the third coordination spheres of the metal ions (see Fig. 8a). As expected, the active MOs correspond to the in-phase and out-of-phase linear combinations of the d-type orbitals of the Cu atoms (see Fig. 8b).

As a consequence of the δ-type overlap between the magnetic orbitals, the antiferromagnetic behavior is much weaker than in acetate analogs. Indeed the singlet-triplet energy difference corresponding to $2J$ is calculated at this CAS-CI level $-2.5\ cm^{-1}$. Using the DDCI-1 iterated set of MOs to dispose of the arbitrariness of the initial set (i.e., singlet versus triplet MOs), the singlet–triplet energy differences were then computed at the DDCI-3 level to be -98 and $-21\ cm^{-1}$ for **1** and **2**, respectively. Despite a 30% deviation from the experimental values, the antiferromagnetic behavior is clearly identified, suggesting a stronger cooperativity in complex **1** than in **2**. The on-site repulsion U was extracted from our calculations and turns out to be ∼60 000 cm^{-1} for both systems, in agreement with previous calculations [40]. In contrast, the resonance integrals is significantly reduced ($t_1 = 1.7 \times 10^3\ cm^{-1}$ and $t_2 = 0.8 \times 10^3\ cm^{-1}$ for **1** and **2**, respectively) as the number of sulfonamide ligands in the complex increases.

At this stage one may question how much the accumulation of bioactive ligands is likely to compete with the metal–metal cooperativity probed by the magnetic interactions. X-ray diffraction and

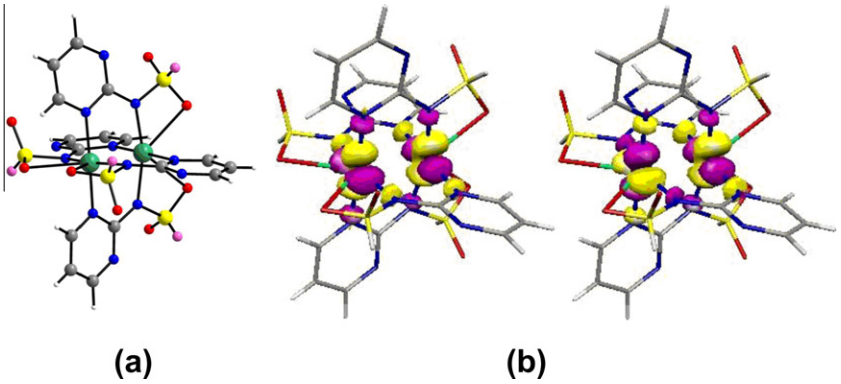

Fig. 8. (a) Simplified structure of **1** used for the *ab initio* calculations. CH_3 groups were replaced by hydrogen atoms with adapted C–H bond lengths (pink). A similar structural simplification was used for **2**; (b) triplet active orbitals from CAS[2,2] calculations performed on **1** and corresponding to the in-phase and out-of phase combinations of the d-type orbitals localized on the Cu(II) center. A similar picture holds for **2**. (Color online.)

cyclic voltammetry studies suggest that the bioactive part of the sulfonamide ligands remains non-coordinated within the complexes structures (dimers and chain). This is the particular specification we wanted to achieve, binding bioactive and accessible ligands to antiseptic Cu(II) metal centers. Besides, magnetic measurements combined with *ab initio* calculations demonstrate a much stronger metal–metal interactions in complexes **1** and **2** than in the polymer analog **1′**.

In order to try out the correlation between metal–metal communication and bioactivity, preliminary antibacterial studies were finally undertaken.

The antibacterial activity of bioactive sulfonamide which are structurally similar to *p*-aminobenzoic acid (PABA) is due to their ability to interfere with the conversion of PABA to dihydrofolate (DHF = folate) by an inhibitory competition with the enzyme dihydropteroate synthetase (DHPS) [41]. The reaction between **1′** (chain) and *E. faecalis* exhibits a MIC which falls down to a value *ca.* 16 mg L^{-1} (HL1: MIC > 128 mg L^{-1}) while complexes **1** and **2** (dimers) are as active as the isolated ligands HL1 (MIC > 128 mg L^{-1}) and HL2 (MIC > 128 mg L^{-1}). Therefore, the absence of communication between the Cu(II) centers in **1′** questions the need for interacting Cu(II) centers in polynuclear bioactive ligand-based structures to ever enhance the antibacteriological activity. The results of the strategies that we have developed, namely (i) increasing the number of sulfonamide ligands within the complex, and (ii) introducing a spacer ligand such as bipyridine between the Cu(II) ions seems to give priority to the second approach in order to tailor antibacteria agents.

4. Conclusion

Following a synthetic strategy to prepare bioactive sulfonamide ligand-based architectures, dinuclear coordination compounds and 1D polymer using Cu(II) antiseptic ions were isolated, characterized and electrochemically investigated. Depending on the synthetic conditions, one can generate different Cu(II):ligand stoichiometries which form single crystals. The combination of electrochemical measurements and single crystal X-ray diffraction supports that (i) the coordination of the sulfonamide ligands to the Cu(II) centers is not altered when dissolution occurs, and (ii) the crucial amino group remains accessible (i.e., non-coordinated) for bioactivity. Using magnetic susceptibility measurements in contact with *ab initio* calculations, a rather strong antiferromagnetic behavior is observed in both dinuclear compounds while the cooperativity as measured through the effective hopping integral is reduced as the number of sulfonamide ligands increases. Despite this apparent drawback, the bioactivity towards *E. faecalis* was measured and reveals that the minimum inhibitory concentrations in **1** and **2** are comparable to those of the isolated ligands. These preliminary bacteriological studies demonstrate that the bioactive efficiency is maintained in these sulfonamide based Cu(II) complexes. By preserving the structure of the bioactive ligand and allowing for communication between the Cu(II) centers, the targeted dinuclear species **1** and **2** fulfill the reported specifications found in the literature. Nevertheless, our results question the prerequisite for cooperative metal centers to rationally design antibacterial agents since the minimum inhibitory concentration in the paramagnetic chain **1′** is greatly reduced.

Acknowledgment

Single-crystal X-ray diffraction studies were performed at the "Centre de Diffractométrie Henri Longchambon" at Université Claude Bernard Lyon 1.

Appendix A. Supplementary data

CCDC 549111, 827013 and 827014 contain the supplementary crystallographic data for structures of complexes **1**, **2** and **1′**, respectively. An X-ray crystallographic file in CIF format, this material is available free of charge via the Internet at http://www.pubs.acs.org. These data can be obtained free of charge via http://www.ccdc.cam.ac.uk/conts/retrieving.html, or from the Cambridge Crystallographic Data Centre, 12 Union Road, Cambridge CB2 1EZ, UK; fax: (+44) 1223-336-033; or e-mail: deposit@ccdc.cam.ac.uk.

References

[1] L.-J. Ming, Med. Res. Rev. 23 (2003) 697.
[2] M.S. Iqhal, A.H. Khan, B.A. Loothar, I.H. Bukkari, Med. Chem. Res. 18 (2009) 31.
[3] B.M. Macias, V. Villa Maria, L. Sanchez-Mesonero, F. Sanz, J. Borras, M.Z. Gonzalez-Alvarez, Anorg. Allg. Chem. (2007) 1937.
[4] (a) E. Kremer, G. Facchin, E. Estevez, P. Albores, E.J. Baran, J. Ellena, M.H. Torre, J. Inorg. Biochem. 100 (2006) 1167;
(b) M. Mondelli, V. Brune, G. Borthagaray, J. Ellena, O.R. Nascimento, C. Leite, A.A. Batista, M.H. Torre, J. Inorg. Biochem. 102 (2008) 282.
[5] R. Cejudo, G. Alzuet, M. Gonzalez-Alvarez, J.L. Garcia-Gimenez, J. Borras, M. Liu-Gonzalez, J. Inorg. Biochem. 100 (2006) 70.
[6] (a) K.J. Humpreys, A.J. Jonhson, K.D. Karlin, S.E. Rokita, J. Biol. Inorg. Chem. 7 (2002) 835;
(b) M. Gonzalez-Alvarez, G. Alzuet, J. Borras, M. Pitié, B. Meunier, J. Biol. Inorg. Chem. 8 (2003) 644;
(c) L. Li, K.D. Karlin, S.E. Rokita, J. Am. Chem. Soc. 127 (2005) 520.
[7] I. Beloso, J. Castro, J.A. García-Vázquez, P. Pérez-Lourido, J. Romero, A. Sousa, Polyhedron 25 (2006) 2673.
[8] I. Beloso, J. Borras, J. Castro, J.A. Garcia-Vazquez, P. Perez-Lourido, J. Romero, A. Sousa, Eur. J. Inorg. Chem. 3 (2004) 635.
[9] (a) T.D. Owens, F.J. Hollander, A.G. Oliver, J.A. Elmann, J. Am. Chem. Soc. 123 (2001) 1539;

(b) C. Worch, A.C. Mayer, C. Bolm, in: T. Toru, C. Bolm (Eds.), Organosulfur Chemistry in Asymmetric Synthesis, Wiley-VCH, Weinheim, (2008). P. 209.
[10] (a) M.H. Torre, G. Facchin, E. Kremer, E.E. Castellano, O.E. Piro, E.J. Baran, J. Inorg. Biochem. 94 (2003) 200;
(b) G.M. Golzar Hossain, A.J. Amoroso, A. Banu, K.M.A. Malik, Polyhedron 26 (2007) 967.
[11] J.B. Tommasino, G. Pilet, F. Renaud, D. Luneau, Polyhedron 30 (2011) 1663.
[12] (a) B. Bleaney, K.D. Bowers, Proc. R. Soc. Lond. A 214 (1952) 451;
(b) G.M. Brown, R. Chidambaram, Acta Crystallogr., Sect. B 29 (1973) 2393.
[13] CRYSALISPRO, Oxford Diffraction Ltd., Version 1.171.33.46 (release 27-08-2009 CrysAlis171 .NET).
[14] CRYSALISPRO, Oxford Diffraction Ltd., Version 1.171.33.46 (release 27-08-2009 CrysAlis171 .NET); Empirical absorption correction using spherical harmonics, implemented in SCALE3 ABSPACK scaling algorithm.
[15] J. De Meulenaar, H. Tompa, Acta Crystallogr., Sect. A 19 (1965) 1014.
[16] G. Cascarano, A. Altomare, C. Giacovazzo, A. Guagliardi, A.G.G. Moliterni, D. Siliqi, M.C. Burla, G. Polidori, M. Camalli, Acta Crystallogr., Sect. A 52 (1996) C-79.
[17] D.J. Watkin, C.K. Prout, J.R. Carruthers, P.W. Betteridge, CRISTAL Issue 11, Chemical Crystallography Laboratory, Oxford, UK, 1999.
[18] P. Pascal, Ann. Chim. Phys. 19 (1910) 5.
[19] Matlab, The MathWorks Inc., 2000.
[20] Optimiseur-Visialiser, EPFL, Lausanne, 2001.
[21] (a) S. Messaoudi, V. Robert, N. Guihéry, D. Maynau, Inorg. Chem. 45 (2006) 3212;
(b) J.-B. Rota, L. Norel, C. Train, N. Ben Amor, D. Maynau, V. Robert, J. Am. Chem. Soc. 130 (2008) 10380.
[22] MOLCAS7: The Next Generation, J. Comp. Chem. 31 (2010) 224. Available from: <dx.doi.org/10.1002/jcc.21318/>.
[23] B.O. Roos, R. Lindh, P.-A. Malmqvist, V. Veryazov, P.-O. Widmark, J. Phys. Chem. A 109 (2005) 6575.
[24] (a) J. Miralles, O. Castell, R. Caballol, J.-P. Malrieu, Chem. Phys. 172 (1993) 33;
(b) N. BenAmor, D. Maynau, Chem. Phys. Lett. 286 (1998) 211.
[25] N. Guihéry, V. Robert, F. Neese, J. Phys. Chem. A 112 (2008) 11979.
[26] J. Bonner, M. Fisher, Phys. Rev. 135 (1964) 640.
[27] S. Shova, G. Novitchi, M. Gdaniec, A. Caneschi, D. Gatteschi, L. Korobchenko, V.K. Voronkova, Y.A. Simonov, C. Turta, Eur. J. Inorg. Chem. (2002) 3313.
[28] Y. Deng, J. Liu, B. Wu, C. Ambrus, T. Keene, O. Waldmann, S. Liu, S. Decurtins, X. Yang, Eur. J. Inorg. Chem. (2008) 1712.
[29] R. Feyerherm, S. Abens, D. Gunther, T. Ishida, M. Meissner, M. Meschke, T. Nogami, M. Steiner, J. Phys.: Condens. Matter 12 (2000) 8495.
[30] S. Eggert, I. Affleck, M. Takahashi, Phys. Rev. Lett. 73 (1994) 332.
[31] M. Julve, M. Verdaguer, J. Faus, F. Tinti, J. Moratal, A. Monge, E. Gutierrez-Puebla, Inorg. Chem. 26 (1987) 3520.
[32] S.T. Ochsenbein, F. Tuna, M. Rancan, R.S.G. Davies, C.A. Muryn, O. Waldmann, R. Bircher, A. Sieber, G. Carver, H. Mutka, F. Fernandez-Alonso, A. Podlesnyak, L.P. Engelhardt, G.A. Timco, H.U. Gudel, R.E.P. Winpenny, Chem. Eur. J. 14 (2008) 5144.
[33] S. Cabaleiro, R. Calvo, J. Castro, A. Garcia-Vazquez, L.M.B. Napolitano, O.R. Nascimento, P. Perez-Lourido, J. Romero, A. Sousa, J. Chem. Crystallogr. 38 (2008) 71.
[34] R. Cejudo-Marin, G. Alzuet, S. Ferrer, J. Borras, A. Castineiras, E. Monzani, L. Casella, Inorg. Chem. 43 (2004) 6805.
[35] J. Casanova, G. Alzuet, J. Latorre, J. Borras, Inorg. Chem. 36 (1997) 2052.
[36] J. Ellena, E. Kremer, G. Facchin, E.J. Baran, O.R. Nascimento, A.J. Costa-Filho, M.H. Torre, Polyhedron 26 (2007) 3277.
[37] A. Bodoki, G. Alzuet, A. Hangan, L. Oprean, F. Estevan, A. Castineiras, J. Borras, Inorg. Chim. Acta 363 (2010) 3139.
[38] L. Gutierrez, G. Alzuet, J. Borras, A. Castineiras, A. Rodriguez-Fortea, E. Ruiz, Inorg. Chem. 40 (2001) 3089.
[39] C.J. Calzado, J. Cabrero, J.-P. Malrieu, R. Caballol, J. Chem. Phys. 116 (2002) 3985.
[40] J.B. Rota, B. Le Guennic, V. Robert, Inorg. Chem. 49 (2010) 1230.
[41] (a) G.M. Brown, Adv. Biochem. 35 (1971) 35;
(b) G.H. Miller, P.H. Doukas, J.K. Seydal, J. Med. Chem. 15 (1972) 700.